Magnetic Properties of Low-Dimensional α and γ CoV2O6

ARTICLE *in* THE JOURNAL OF PHYSICAL CHEMISTRY C · SEPTEMBER 2011

Impact Factor: 4.77 · DOI: 10.1021/jp2053772

THE JOURNAL OF PHYSICAL CHEMISTRY C

ARTICLE

pubs.acs.org/JPCC

Magnetic Properties of Low-Dimensional α and γ CoV_2O_6

M. Lenertz, J. Alaria, D. Stoeffler, S. Colis,* and A. Dinia

Institut de Physique et Chimie des Matériaux de Strasbourg (IPCMS), UMR 7504 CNRS and University of Strasbourg (UDS-ECPM), 23 rue du Loess, BP 43, F-67034 Strasbourg Cedex 2, France

ABSTRACT: In this work, we analyze the magnetic properties of the low-dimensional CoV_2O_6 powders showing monoclinic (α) and triclinic (γ) crystalline structures. The two phases are constituted of parallel 1D Co chains organized in planes that are separated by vanadium oxide thin layers. Both α and γ phases are antiferromagnetic in the ground state with Néel temperatures of 15 and 7 K, respectively. The magnetization curves recorded at 5 (α phase) and 1.8 K (γ phase) show a stepped variation with sharp field-induced magnetic transitions and a magnetization plateau at one-third of the saturation magnetization. In α-CoV_2O_6, additional steps are evidenced when the temperature decreased from 5 to 1.8 K. This is accompanied by an increasing hysteresis corresponding to the magnetic field transitions. From the magnetization curves recorded at different temperatures, a magnetic phase diagram could be determined. The estimated Co moment is large and reaches in the α and γ phases 4.5 and 3 μ_B, respectively, suggesting the existence of an orbital contribution in α-CoV_2O_6.

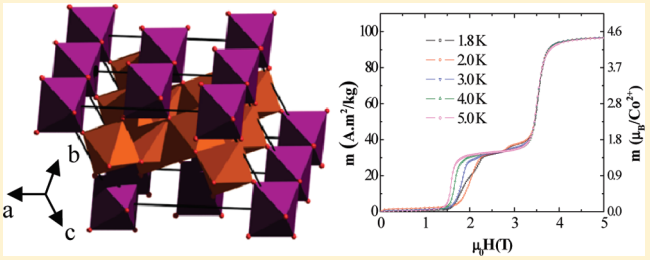

I. INTRODUCTION

Low-dimensional magnetic oxides attract an increasing interest from the scientific community because of their peculiar magnetic properties related to their crystalline structure.[1−3] Their structure is usually composed of linear magnetic chains[4] or planes.[5] Consequently, such compounds exhibit unusually strong magnetic anisotropies and stepped magnetization variations corresponding to magnetic field-induced transitions. These compounds are a perfect playground to investigate the properties of quasi-1D magnets in inorganic materials with transitions at relatively low magnetic field. Moreover, strong correlation between electronic and magnetic properties could offer the possibility to investigate new spin-dependent transport phenomena such as two-stage magnetoresistance observed in metallic compounds.[6] With respect to classic multilayered systems where magnetoresistance is strongly related to the interdiffusion at the interfaces,[7,8] such oxides integrate naturally both the magnetic and nonmagnetic subsystems, thus avoiding any interdiffusion related phenomena. In the case of insulating materials, these systems could be used for spin filtering as insulating barriers leading to a nearly fully spin polarized current that could be efficiently injected in semiconductors.[9]

Among these oxides, CoV_2O_6 was first studied to describe its crystalline structure.[10−13] According to the CoO-V_2O_5 phase diagram,[10,11] the cobalt vanadium oxide CoV_2O_6 presents two allotropic phases depending on whether the synthesis is carried out below or above 680 °C. The high-temperature phase presents a brannerite-like monoclinic structure with the $C2/m$ space group, often called α phase (Figure 1a). The lattice parameters of α-CoV_2O_6 are a = 9.251 Å, b = 3.504 Å, c = 6.618 Å, and β = 111.64°.[11] The low-temperature phase, also called γ phase, presents a triclinic structure with the P-1 space group (Figure 1b) and the lattice parameters a = 7.164 Å, b = 8.872 Å, c = 4.806 Å, α = 90.29°, β = 93.66°, and γ = 102.05°.[13] Both phases are constituted of edge-connected CoO_6 octahedra forming 1D chains along the b axis. The intrachain Co−Co distance is 3.504 and 2.976 Å in the α and γ phases, respectively. For both phases, the chains form magnetic bidimensional layers separated by a nonmagnetic vanadium oxide layer. This layer is composed of zigzag chains of edge-connected VO_6 octahedra parallel to the Co chains (i.e., the b direction). In the α phase, the vanadium chains are directly connected to one another, and the zigzag is in the ab plane. In the γ phase, the zigzag occurs perpendicular to the bc plane, and the chains are connected through VO_4 tetrahedra. The distance between the Co chains is 4.626 Å for the α phase and 4.806 Å for the γ one.

Further studies focused on the electrochemical,[14] catalytic,[15] and magnetic properties of CoV_2O_6. An antiferromagnetic ordering was evidenced by recording the variation of the magnetic susceptibility with temperature.[16] More recent studies showed that the magnetization curves recorded at 5 K on α-CoV_2O_6 present a plateau corresponding to one-third of the saturation magnetization (M_S/3) and a strong anisotropy.[17] Similar results were also obtained in γ-CoV_2O_6, but the magnetization plateau at M_S/3 is less defined.[18] Moreover, the magnetization field-induced transition was observed at lower field (∼0.3 T) with respect to that observed in the α phase (1.5 T). However, to our knowledge, there is no uniform picture of the magnetic properties of the two CoV_2O_6 phases, and several studies are far from being complete. For example, the α-CoV_2O_6 phase was never studied below 5 K, although, as it will be shown in the present Article, additional plateaus appear when the temperature

Received: June 8, 2011
Revised: July 25, 2011
Published: July 26, 2011

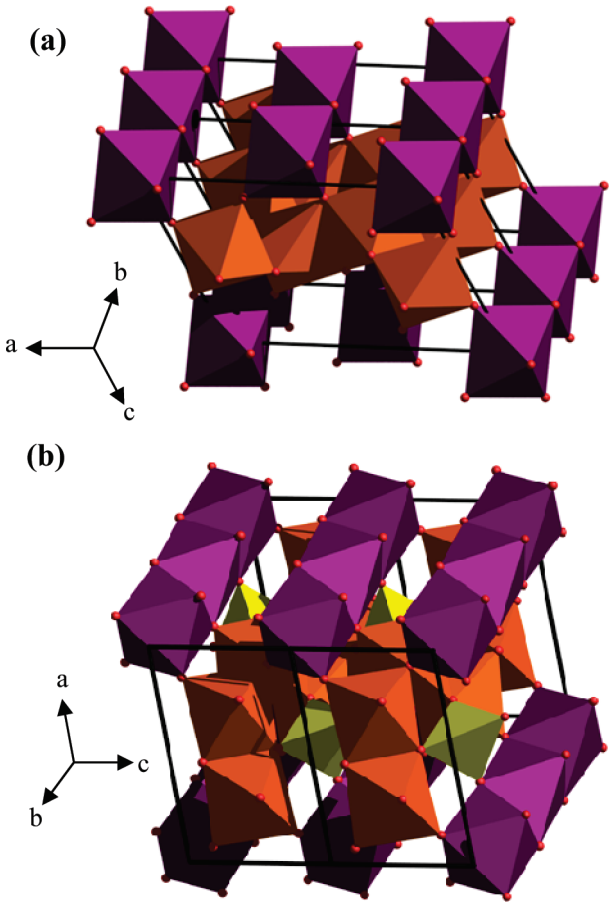

Figure 1. Double unit cell of (a) α-CoV_2O_6 and (b) γ-CoV_2O_6. In violet, brown, and dark yellow are represented the CoO_6 octahedra, VO_6 octahedra, and VO_4 tetrahedra, respectively.

is decreased below 5 K. Therefore, the aim of our work is to give a consistent picture of the temperature- and field-dependent magnetic properties for the two phases of CoV_2O_6.

To clarify the nomenclature used to describe the two different allotropic phases called here α and γ CoV_2O_6, we summarize in Table 1 the different reported studies and analysis techniques used to characterize these samples. It appears clearly from this Table that the phase denomination is not systematically reported, and the same phase can have different names. (See, for instance, ref 19, which calls the γ phase β-CoV_2O_6, or refs 15−18, which speak of CoV_2O_6 without naming exactly the allotropic studied phase.) Here we choose to call the high- and low-temperature phases α and γ, respectively, because these are the original and most widespread nomenclatures used to call these phases.

II. EXPERIMENTAL DETAILS

CoV_2O_6 was prepared by solid-state reaction from vanadium oxide (V_2O_5) and hydrated cobalt oxalate ($CoC_2O_4 \cdot 2H_2O$). A stoichiometric mixture was ground in an agate mortar. To obtain the α-CoV_2O_6 phase, the mixture was heated in air at 720 °C during 40 h in a platinum crucible. The resulting powder was quenched by removing the crucible from the furnace. For the γ-CoV_2O_6 phase, the mixture was heated in air at 620 °C during 45 h and then cooled to room temperature at a rate of 2 °C/min. This resulting powder was ground, pressed into pellets, and heated again at 620 °C during 45 h. Note that the γ phase is stable up to ∼660 °C and that the α phase can be easily frozen by quenching the sample down to room temperature. It is therefore possible to transform the γ phase into the α phase by heating it for several hours at 720 °C. In reverse order, it is possible to obtain from the α phase the γ phase by heating the sample for 20 h at 660 °C.[11]

Table 1. Synthesis of the Different Studies Carried out on CoV_2O_6 Showing the Nomenclature Used for the α and γ Phases and the Analyzes Performed in Each Case

reference	studied phase	denomination of: α-phase	denomination of: γ-phase	characterization
10	α and γ	H-$Co(VO_3)_2$	L-$Co(VO_3)_2$	CoO-V_2O_5 phase diagram
11	α and γ	α-CoV_2O_6	γ-CoV_2O_6	CoO-V_2O_5-MoO_3 phase diagram thermal stability of α- and γ-CoV_2O_6 structure of α-CoV_2O_6
12	α	α-CoV_2O_6	/	structure of α-CoV_2O_6
13	γ	/	γ-CoV_2O_6	synthesis of γ-CoV_2O_6 single crystals structure of γ-CoV_2O_6
14	α and γ	α-CoV_2O_6	γ-CoV_2O_6	electrochemical properties vs Li XRD at different temperatures
15	α	CoV_2O_6	/	catalytic properties XPS spectroscopy
16	α	CoV_2O_6	/	magnetic properties (M vs T)
17	α	CoV_2O_6	/	synthesis of α-CoV_2O_6 single crystals magnetic properties (M vs H, M vs T)
18	γ	/	CoV_2O_6	magnetic properties (M vs H, M vs T)
19	γ	/	β-CoV_2O_6	structure of γ-CoV_2O_6

dx.doi.org/10.1021/jp2053772 |J. Phys. Chem. C 2011, 115, 17190–17196

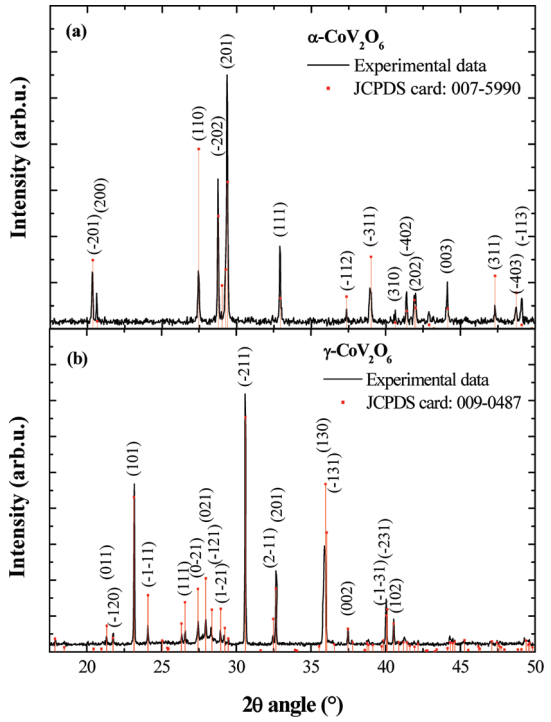

Figure 2. X-ray diffraction patterns for (a) α-CoV_2O_6 and (b) γ-CoV_2O_6 powders synthesized by solid-state reaction. In red are given the patterns as reported in the ICDD database.[20]

The phase purity was checked using a D8 Brücker-AXS X-ray diffractometer equipped with a monochromatic Cu $K\alpha_1$ source (1.54056 Å) and an energy filtered detection. All diffractograms were recorded in standard Bragg−Brentano configuration. The magnetic properties were analyzed using a MPMS SQUID-VSM (Quantum Design) magnetometer in a temperature and field range of 1.8−300 K and 0−7 T, respectively. The temperature dependence variation of the magnetization was carried out under a magnetic field of 0.1 T after the sample was cooled in a field of 0.1 T (FC: field cooling) or in zero field (ZFC: zero field cooling). Previous to any magnetic measurement, all powders were magnetically "aligned" in a polymeric gel that freezes the particle orientation below ∼30 °C. The alignment was performed in a field of 7 T.

III. RESULTS AND DISCUSSION

Figure 2 shows the XRD diffractograms recorded for the α and γ CoV_2O_6 phases. Both samples show the expected lines[20] with no traces of spurious phases in the detection limit of the XRD technique. This let us think that the magnetization measurements that will be presented in the following should not suffer from pollution with other magnetic phases. Moreover, as the powders were aligned in large magnetic fields (7 T), the magnetic moment determined from the magnetization data should be similar to the one measured in single-crystal samples.[17]

A. α-CoV_2O_6. The magnetic properties of α-CoV_2O_6 were first checked using temperature-dependent magnetization variations. The ZFC and FC curves recorded in constant field of 0.1 T (Figure 3) are perfectly superimposed and show a maximum at ∼15 K. Below this temperature, the magnetization decreases to become negligible for temperatures <6 K. This variation shows an antiferromagnetic character for α-CoV_2O_6. Above 15 K,

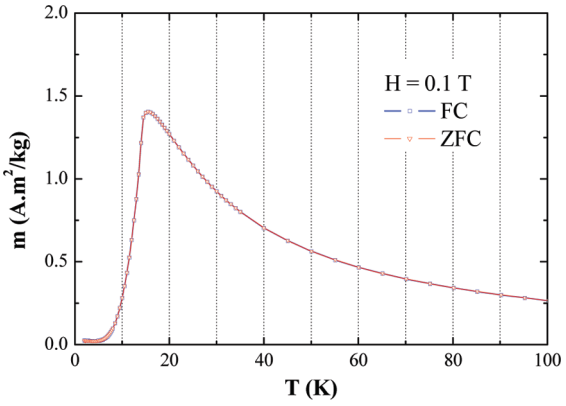

Figure 3. ZFC/FC temperature-dependent magnetization curves recorded at constant field of 0.1 T showing the antiferromagnetic order in α-CoV_2O_6. The Néel temperature is of ∼15 K, which corresponds to the antiferromagnetic−paramagnetic transition.

which corresponds to the Néel temperature of the system, α-CoV_2O_6 becomes paramagnetic, and the magnetization decreases progressively.

To get further details on the magnetic properties of α-CoV_2O_6, we report the first magnetization curves recorded at different temperatures in Figure 4a,b. The magnetization curve at 5 K shows a stepped variation of the magnetization (Figure 4a). Up to 1.5 T, the sample presents almost no magnetic signal, in agreement with the antiferromagnetic behavior evidenced by the $m-T$ variation. At 1.5 T, the onset of the first field-induced magnetization transition is observed. Between 1.9 and 3.2 T, a stable magnetic moment with a value of 1.5 μ_B/Co atom is reached. By further increasing the field, a second magnetization step is observed. The saturation moment of ∼4.5 μ_B/Co atom is reached for 4 T. Therefore, the intermediate magnetization value appears to be 1/3 of the saturation magnetization. This is similar to what was observed in magnetically frustrated oxides with triangular structures such as $Ca_3Co_2O_6$.[21] It is important to note that the magnetic moment of 4.5 μ_B/Co atom is much larger than the expected value for a high spin Co^{2+} ion ($3\mu_B$). This suggests that the magnetic moment has not only a pure spin origin but also an orbital component. It is also interesting to point out that the antiferromagnetic ground state, accompanied by two plateaus in the magnetization curve at 5 K is in agreement with what was previously reported in α-CoV_2O_6 single crystals.[17] According to this study, the easy magnetization axis lies along the c axis of the monoclinic structure, that is, perpendicular to the chains. This is somehow peculiar because the anisotropy measurements in compounds presenting Ising-like chains along the c axis and frustrations in the ab plane[4,6,22] indicate that the easy magnetization axis is parallel to the chains. Surprisingly, this easy magnetization axis is perpendicular to the Co chain direction. This behavior is, however, not well understood and is believed to originate from the competition between the antiferromagnetic interaction between the chains and the ferromagnetic interaction between Co ions usually existing inside the Ising magnetic chains.[17] Indeed, in the ab plane of the α-CoV_2O_6 phase (Figure 1a), two adjacent chains (aligned along the b axis) are shifted one another by half of the in-chain distance between the Co ions. This means that in the ab plane, isosceles triangles are formed between the Co ions of two adjacent chains, and the magnetic frustration appears in the same way because this is observed in triangular lattice-based compounds.[23]

dx.doi.org/10.1021/jp2053772 |J. Phys. Chem. C 2011, 115, 17190–17196

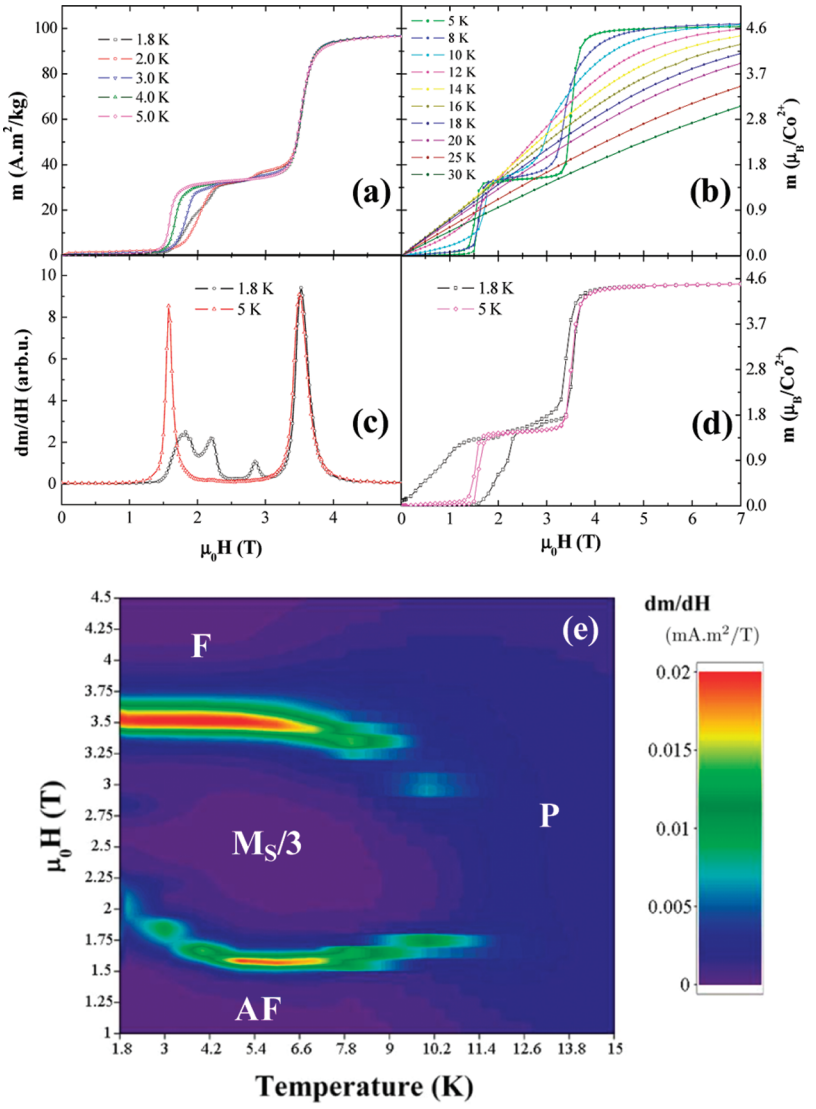

Figure 4. First magnetization curves of α-CoV_2O_6 recorded while increasing the field from zero to saturation for temperatures below (a) and above (b) 5 K. Derivate of the first magnetization curve recorded at 1.8 and 5 K (c) and extrapolated for all temperatures between 1.8 and 15 K (e). (d) Magnetization hysteresis loop recorded at 1.8 and 5 K.

Note also that a change of the easy magnetization axis can be obtained by vacancies that induce distortions in the original crystalline structure.[24]

For temperatures larger than 5 K, the magnetization plateaus disappear progressively. At 14 K and above, the magnetization curve corresponds to a paramagnetic behavior, in agreement with the Néel temperature evidenced by the $m-T$ measurements. As for temperatures below 5 K, the magnetization curves show additional plateaus with respect to those observed at 5 K. This is clearly evidenced by the derivate of the magnetization curve at 1.8 K reported in Figure 4c, where field-induced transitions appear at 1.8, 2.2, 2.8, and 3.5 T. These plateaus, reported here for the first time in CoV_2O_6, were observed in other 1D magnetic systems such as $Ca_3Co_2O_6$. They were attributed to a quantum tunneling effect of the magnetization (QTM)[21] or to combined effects of the magnetic correlations and frustrations.[25,26] Although in $Ca_3Co_2O_6$ the magnetization steps are separated by fixed field intervals of 1.2 T, in our case these steps do not appear at regular field values. This observation may suggest that

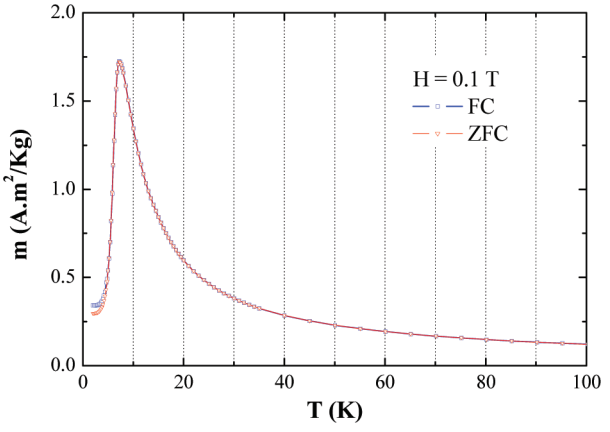

Figure 5. ZFC/FC temperature-dependent magnetization curves recorded at constant field of 0.1 T showing the antiferromagnetic order in γ-CoV_2O_6. The Néel temperature is ∼7 K, which corresponds to the antiferromagnetic−paramagnetic transition.

dx.doi.org/10.1021/jp2053772 |J. Phys. Chem. C 2011, 115, 17190–17196

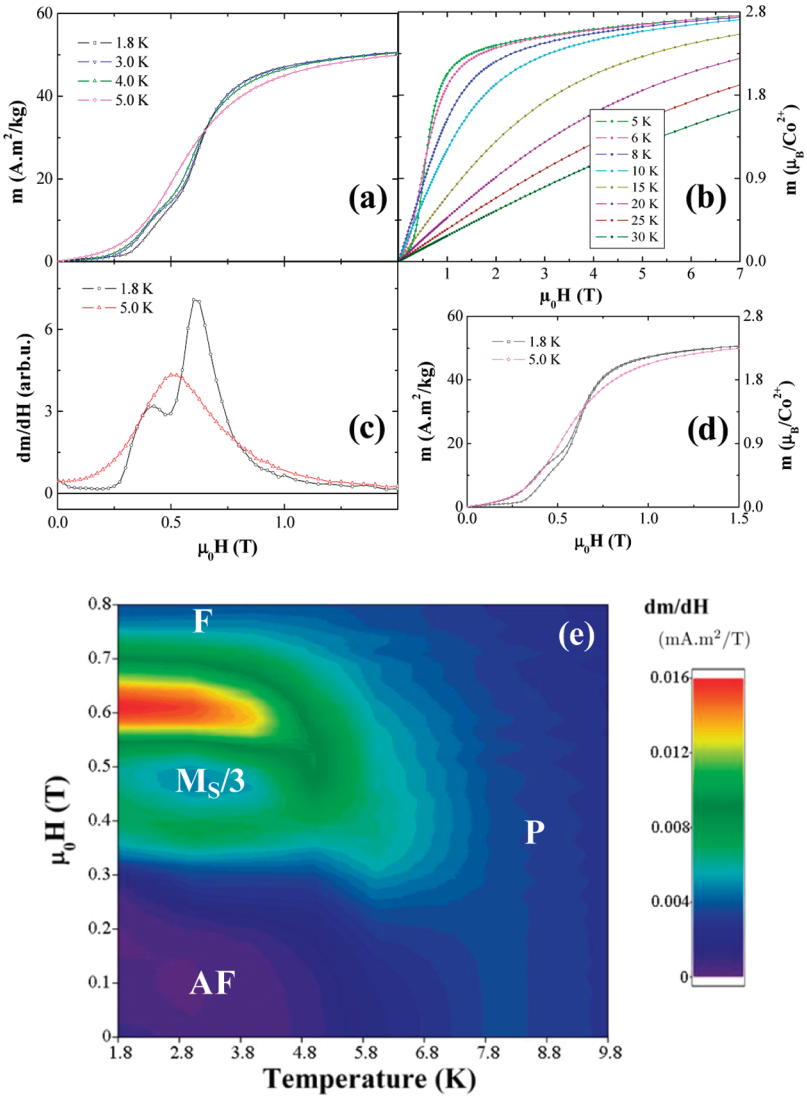

Figure 6. First magnetization curves of γ-CoV_2O_6 recorded while increasing the field from zero to saturation for temperatures below (a) and above (b) 5 K. Derivate of the first magnetization curve recorded at 1.8 and 5 K (c) and extrapolated for all temperatures between 1.8 and 10 K (e). (d) Magnetization hysteresis loop recorded at 1.8 and 5 K.

the origin of the steps may not be due to QTM but to the magnetic frustrations existing in the system. It is interesting to point out that the position of the magnetization steps depends on the temperature. (See Figure 4e.) Indeed, the field window between the two main field-induced magnetization transitions decreases while we move away from 5 K either by increasing or decreasing the temperature. This suggests that the magnetization reversal processes are thermally assisted. The thermally assisted character of the magnetization reversal can also be evidenced by the presence of a strong hysteresis in the magnetization loop. Whereas at 5 K, this hysteresis is small (and completely absent at higher temperatures), at 1.8 K, the hysteresis is particularly large, especially in the case of the first field-induced magnetization transition (~1.6 T) (Figure 4d). Finally, it is noteworthy to mention that the map of the magnetization derivate as a function of field and temperature (Figure 4e) constitutes also a magnetic phase diagram for α-CoV_2O_6. In this diagram, the lower (μ_0H < 1.5 T) and the upper (μ_0H > 3.5 T) regions correspond to the antiferromagnetic (AF) and ferromagnetic (F) phases, respectively, and are separated by the circular-like zone corresponding to the 1/3 of the saturation magnetization (M_S/3). For temperatures >13 K, the sample appears to be mostly paramagnetic (P).

B. γ-CoV_2O_6. The ZFC and FC curves recorded for γ-CoV_2O_6 are shown in Figure 5. The magnetic behavior is similar to the one observed for α-CoV_2O_6; that is, the main magnetic interactions are antiferromagnetic. The Néel temperature is, however, lower in this case, with a value of ~7 K, which suggests a weaker interaction between the magnetic moments. This is also consistent with the higher magnetization value corresponding to the antiferromagnetic−paramagnetic transition in γ-CoV_2O_6 (Figure 5) than in α-CoV_2O_6 (Figure 3). It is interesting to point out that the larger distance between chains in γ-CoV_2O_6 (4.806 Å) than in α-CoV_2O_6 (4.626 Å) is in agreement with the lower Néel temperature in γ-CoV_2O_6. However, the distance between the Co ions inside the chains is shorter in the γ phase (3.504 Å in α-CoV_2O_6 and 2.976 Å in γ-CoV_2O_6). This suggests that the chains are antiferromagnetically coupled, whereas the Co moments inside a chain are ferromagnetically coupled.

dx.doi.org/10.1021/jp2053772 |J. Phys. Chem. C 2011, 115, 17190–17196

The lower antiferromagnetic interaction between the magnetic moments inside γ-CoV_2O_6 is also well-visible in the magnetization curves recorded at different temperatures (Figure 6a,b). Although the magnetization curve shows two steps as this was observed in α-CoV_2O_6 (Figure 4a,c), the fields at which these magnetic transitions occur are only of 0.42 and 0.61 T (Figure 6c). Another important feature of the magnetization curve recorded at 1.8 K is the small positive slope in the low ($\mu_0 H < 0.25$ T, Figure 6a) and high ($\mu_0 H > 3$ T, Figure 6b) magnetic field regimes. The slope in the low-field regime may suggest a lower anisotropy, which should lead to a low saturation field. However, saturation is not reached even for fields as large as 7 T. To explain the large saturation field, one should rather look into the details of the crystalline structure of γ-CoV_2O_6. With respect to the α phase in which the Co ions are perfectly aligned inside the chains, in γ-CoV_2O_6, a canting angle exists between the directions of two adjacent Co−Co bonds. This is due to the fact that although Co is always in octahedral coordination, it belongs to two crystallographically independent sites that alternate in the sequence 122122.[27] This chain distortion also leads to two types of magnetic interactions inside a chain. Along with this distortion, it is therefore possible that the local anisotropy has slightly different orientations with respect to the average anisotropy axis. Under these conditions, the small slope of the magnetization in the high-field regime corresponds to the progressive rotation of the magnetic moments from the local anisotropy axis to the average anisotropy axis, that is, the field direction in our case. Note also that the existence of the canting angle may also explain the much smaller hysteresis in the magnetization curve at 1.8 K in the γ phase (Figure 6d). Indeed, the existence of an angle between different local easy magnetization axes can trigger the rotation of the magnetic moments toward the antiferromagnetic configuration while decreasing the magnetic field.

Another important observation is that the magnetization of γ-CoV_2O_6 at 7 T leads to a magnetic moment of 2.8 μ_B/Co atom. Given the small slope of the magnetization curve in the high field regime and that Kimber et al.[18] obtained 2.9 μ_B/Co atom at 9 T, it is reasonable to assume that the saturation magnetization is ~3 μ_B/Co atom, which is the value expected for high-spin Co^{2+} ion. With respect to α-CoV_2O_6, it appears therefore that in γ-CoV_2O_6 the orbital magnetic moment, if it exists, is very small, which is consistent with the octahedral environment of the Co ions. An intriguing question that remains open is why Co in CoO_6 octahedra presents in α-CoV_2O_6 an orbital moment of 1.5 μ_B/Co atom whereas in γ-CoV_2O_6 the orbital moment is very small. One may think at the canting angle in the γ phase, although precise calculations should be carried out.

The magnetic phase diagram of γ-CoV_2O_6 obtained from the derivate of the magnetization curves at different temperatures (Figure 6e) is similar to the one of α-CoV_2O_6 (Figure 4e). The only differences are related to the lower ordering temperature (~6 K), above which the sample becomes paramagnetic and to the less visible first magnetization step at ~0.45 T. The plateau at 1/3 of the saturation magnetization between 0.45 and 0.6 T is also much less evidenced.

IV. CONCLUSIONS

In conclusion, we have studied the magnetic properties of monoclinic (α) and triclinic (γ) CoV_2O_6 with an emphasize on the magnetic differences between the two phases and the relation between magnetism and crystalline structure. Both phases are antiferromagnetic in the ground state with ordering temperatures of 15 and 7 K, respectively. Although both phases are composed of chains of Co situated in octahedral sites, the magnetic moment of Co in the two phases is different mainly due to the spin orbit coupling. The orbital component of the Co magnetic moment is 1.5μ_B in the α phase, whereas it is negligible in γ-CoV_2O_6. This is probably related to distortions of the chains in the γ phase. Through temperature- and field-dependent magnetic measurements, the magnetic phase diagrams have been determined.

AUTHOR INFORMATION

Corresponding Author

*E-mail: colis@ipcms.u-strasbg.fr.

ACKNOWLEDGMENT

We acknowledge the support of the French Agence Nationale de la Recherche (ANR) under the reference ANR-09-BLAN-0187-03.

REFERENCES

(1) Schiffer, P. *Nature* **2002**, *420*, 35.
(2) Kodama, K.; Takigawa, M.; Horvatic, M.; Berthier, C.; Kageyama, H.; Ueda, Y.; Miyahara, S.; Becca, F.; Mila, F. *Science* **2002**, *298*, 395.
(3) Coldea, R.; Tennant, D. A.; Wheeler, E. M.; Wawrzynska, E.; Prabhakaran, D.; Telling, M.; Habicht, K.; Smeibidl, P.; Kiefer, K. *Science* **2010**, *327*, 177.
(4) Moubah, R.; Colis, S.; Ulhaq-Bouillet, C.; Drillon, M.; Dinia, A. *J. Mater. Chem.* **2008**, *18*, 5543.
(5) Moubah, R.; Colis, S.; Ulhaq-Bouillet, C.; Schmerber, G.; Viart, N.; Drillon, M.; Dinia, A.; Muller, D.; Grob, J. J. *Eur. Phys. J. B* **2008**, *66*, 315.
(6) Ishiwata, S.; Terasaki, I.; Ishii, F.; Nagaosa, N.; Mukuda, H.; Kitaoka, Y.; Saito, T.; Takano, M. *Phys. Rev. Lett.* **2007**, *98*, 217201.
(7) Colis, S.; Gieres, G.; Bär, L.; Wecker, J. *Appl. Phys. Lett.* **2003**, *83*, 948.
(8) Fix, T.; Barla, A.; Ulhaq-Bouillet, C.; Colis, S.; Kappler, J. P.; Dinia, A. *Chem. Phys. Lett.* **2007**, *434*, 276.
(9) Filip, A. T.; LeClair, P.; Smits, C. J. P.; Kohlhepp, J. T.; Swagten, H. J. M.; Koopmans, B.; de Jonge, W. J. M. *Appl. Phys. Lett.* **2002**, *81*, 1815.
(10) Brisi, C. *Ann. Chim. (Rome, Italy)* **1957**, *47*, 815.
(11) Mocała, K.; Ziółkowski, J.; Dziembaj, L. *J. Solid State Chem.* **1985**, *56*, 84.
(12) Jasper-Tönnies, B.; Muller-Buschbaum, H. K. *Z. Anorg. Allg. Chem.* **1984**, *508*, 7.
(13) Muller-Buschbaum, H.; Kobel, M. *J. Alloys Compd.* **1991**, *176*, 39.
(14) Baudrin, E.; Laruelle, S.; Denis, S.; Touboul, M.; Tarascon, J. M. *Solid State Ionics* **1999**, *123*, 139.
(15) Xu, A.; Lin, Q.; Ji, M.; Zhaorigetu, B. *React. Kinet. Catal. Lett.* **2008**, *93*, 273.
(16) Belaïche, M.; Bakhache, M.; Drillon, M.; Derory, A.; Vilminot, S. *Physica B* **2001**, *305*, 270.
(17) He, Z.; Yamaura, J. I.; Ueda, Y.; Cheng, W. *J. Am. Chem. Soc.* **2009**, *131*, 7554.
(18) Kimber, S. A. J.; Argyriou, D. N.; Attfield, J. P. 2008, arXiv:-0804.2966v1.
(19) International Center for Diffraction Database (ICDD), card number 051-0130 for β CoV_2O_6.
(20) International Center for Diffraction Database (ICDD), card number 007-5990 and 009-0487 for α and γ CoV_2O_6, respectively.
(21) Maignan, A.; Hardy, V.; Hébert, S.; Drillon, M.; Lees, M. R.; Petrenko, O.; Paul, D.; Mc, K.; Khomskii, D. *J. Mater. Chem.* **2004**, *14*, 1231.

(22) Kobayashi, S.; Mitsuda, S.; Ishikawa, M.; Miyatani, K.; Kohn, K. *Phys. Rev. B* **1999**, *60*, 3331.
(23) Kimber, S. A. J.; Attfield, J. P. *Phys. Rev. B* **2007**, *75*, 064406.
(24) Mentré, O.; Kabbour, H.; Ehora, G.; Tricot, G.; Daviero-Minaud, S.; Whangbo, M. H. *J. Am. Chem. Soc.* **2010**, *132*, 4865.
(25) Moubah, R.; Colis, S.; Ulhaq-Bouillet, C.; Drillon, M.; Dinia, A. *J. Phys.: Condens. Matter* **2011**, *23*, 276002.
(26) Soto, R.; Martinez, G.; Baibich, M. N.; Florez, J. M.; Vargas, P. *Phys. Rev. B* **2009**, *79*, 184422.
(27) Kimber, S. A. J.; Mutka, H.; Chatterji, T.; Hofmann, T.; Henry, P. F.; Bordallo, H. N.; Argyriou, D. N.; Attfield, J. P. 2010, arXiv:1008.3927v1.